Available online at www.sciencedirect.com
ScienceDirect
Separation and Purification Technology 59 (2008) 101–107
Separation Purification Technology
www.elsevier.com/locate/seppur

Effect of characteristics of activated carbon on removal of bromate

Winn-Jung Huang [a,*], Yung-Ling Cheng [b]

[a] Department of Environmental Engineering, Hung Kuang University, 34 Chung Chie Road, Sha-Lu, Taichung, Taiwan
[b] Environmental Toxins Laboratory, Hung Kuang University, 34 Chung Chie Road, Sha-Lu, Taichung, Taiwan

Received 18 May 2006; received in revised form 25 May 2007; accepted 29 May 2007

Abstract

This study evaluates how the characteristics of activated carbon (AC) influence the adsorption–reduction of bromate (BrO_3^-) by performing kinetic and isotherm tests. Experimental results reveal that both physical and chemical effects simultaneously affect the adsorption–reduction process. The wood-based carbons contained more mesopores than coconut- and coal-based carbons, resulting in the adsorption of more BrO_3^-. The equilibrium- and maximum-adsorption capacities were calculated as a function of the effect of mesopore volume. The carbon surface chemistry seems to be significant in the adsorption–reduction process. Activated carbons with high pH_{zpc} values and many basic groups exhibit a neutral or positive charge under typical pH conditions, promoting BrO_3^- adsorption–reduction at the carbon surface. The kinetic data obtained from three forms of carbons have been analyzed using three kinetic models—pseudo-first-order, pseudo-second-order and intraparticle diffusion models. Among the kinetic models studied, the intraparticle diffusion was the best applicable model to describe the adsorption of BrO_3^- onto AC.

Keywords: Activated carbon; Bromate; Adsorption kinetic; Adsorption isotherm; Mesopore

1. Introduction

As a genotoxic carcinogen, bromate (BrO_3^-) may be present in drinking water when ozonation is adopted to treat bromide (Br^-)-containing water [1–3]. Bromate can be formed, during ozonation, via a complex mechanism in which molecular ozone (O_3) and hydroxyl radical ($OH^\bullet$) reactions are present [4]. During the chemical oxidation of natural waters that contains Br^- by O_3 and $OH^\bullet$, BrO_3^- is formed at concentrations from 1 to 50 μg/L in full-scale drinking water plants [5–7].

Bromate is an animal carcinogen. The kidney is a target for both BrO_3^--induced toxicity and cancer, the peritoneum for cancer, testes for lowered sperm count and the thyroid for follicular cell cancer [8]. The World Health Organization (WHO) has estimated that the BrO_3^- concentration in drinking water that corresponds to a cancer risk of 10^{-5} (life-time exposure) is 3 μg/L [9]. The USEPA document for ozone and its by-products used the linearized multistage model to estimate 10^{-6}, 10^{-5} and 10^{-4} life-time excess cancer risks of 0.05, 0.5, and 5 μg/L bromate, respectively.

Many works have studied the adsorption by activated carbon (granular or powder) adsorption to remove BrO_3^- from water and have found that it is effective. The BrO_3^- that is removed by activated carbon has been postulated to be adsorbed, reduced to hypobromite (BrO^-) and finally reduced to bromide (Br^-) on the activated carbon surface [10]. The mechanism by which BrO_3^- is removed by activated carbon has also been analyzed by other researchers [11–13], especially with reference to the surface conditions and properties of many forms of activated carbon including granular activated carbon (GAC) and powdered activated carbon (PAC). These researchers have posited that BrO_3^- is reduced by activated carbon according to the following reactions.

$$\equiv C + BrO_3^- \rightarrow BrO^- + \equiv CO_2$$

$$\equiv C + 2BrO^- \rightarrow 2Br^- + \equiv CO_2$$

where ≡C represents the activated carbon surface and $\equiv CO_2$ is a surface oxide.

In bench- and pilot-scale column testing, BrO_3^- has been effectively removed by virgin granular activated carbon (GAC), but the GAC capacity is carbon-specific and depends on the source water [11,12]. Miller et al. [14], for example, adopted energy dispersive X-ray analysis and found that the

* Corresponding author. Tel.: +886 4 26318652x4112; fax: +886 4 26525245.
E-mail addresses: huangwj@sunrise.hk.edu.tw (W.-J. Huang), octling@yahoo.com.tw (Y.-L. Cheng).

1383-5866/$ – see front matter © 2007 Elsevier B.V. All rights reserved.
doi:10.1016/j.seppur.2007.05.034

acid-washing of carbon removed a significant amount of surface metal. Carbon that was only acid-washed did not exhibit improved BrO_3^- reduction, and the presence/absence of surface metals did not affect BrO_3^- reduction. Studebaker [15] found that carbons with less surface oxygen tend to be basic and have an anion exchange capacity because of their positive charge. Therefore, the adsorption of protons by a basic carbon makes the carbon surface more electrostatically attractive to anions. Graham [16] found that the adsorption of an anion decreased as the acidity of the carbon increased, which fact is attributable to unfavorable electrostatic interactions between the anions and the acid groups. Siddiqui et al. [10] studied BrO_3^- adsorption/reduction from solution, but focused only on the surface chemistry of the adsorbent; the authors found a correlation between basic functional groups (or pH_{zpc}) and the maximum amount adsorbed by each adsorbent. Unfortunately, in the latter work, the isotherms were drawn as fitted curves with no actual adsorption data, which would have indicated the precision of the measurements. Additionally, the number of works on the kinetics of activated carbon adsorption to remove BrO_3^- is still limited; works of the effect of the porosity of activated carbon on the adsorption process are particularly few. The adsorption time and capacity for BrO_3^- reduction by activated carbon to satisfactorily low levels at a water treatment plant must be determined.

This work elucidates how the physical and chemical characteristics of carbon influence BrO_3^- removal. The adsorption kinetics and isotherms of three forms of activated carbon are compared. The adsorption kinetics and capacities are related to the characteristics of the carbons. These data reveal the adsorption process in terms of carbon surface chemistry and porosity.

2. Experimental

2.1. Materials

Commercial forms of activated carbon (AC), Norit (AC_N), Calgon (AC_C) and YUB (AC_Y), from various sources were evaluated in kinetic and isotherm experiments. The main characteristics of selected ACs, including raw material, mean particle size, total surface area, iodine number, hardness, abrasiveness, bulk density and ash content, were described by the manufacturers (Table 1). The contents of acid and basic groups were determined using the acid–base titration procedure that was described by Siddiqui et al. [10]. The ACs that were used in the kinetic and isotherm experiments were prepared using the following procedures. Commercial ACs were pulverized and sieved to yield particles with main diameters that correspond to a 230–300 mesh, or a main particle diameter of 65.5 μm. Following sieving, the carbons were washed using deionized water, and baked at 175 °C for 1 week to remove any volatile impurities. They were then placed in an oven at 105 °C. Before use, the carbons were placed in desiccators and then cooled to room temperature.

In a further test of the effects of surface chemistry, the surface chemistry of carbon AC_Y was modified by cautious thermal reduction in an argon environment. The details of this treatment have been presented elsewhere [17]. The reduced samples, AC_Y-T550 and AC_Y-T950, were thermally reduced at 550 and 950 °C for 1 h. Next, the effect of acid treatment on BrO_3^- adsorption was studied. Each form of carbon was immersed in 1 l of 6 M HNO_3 at room temperature. After 24 h, the acid-treated carbons were thoroughly rinsed with distilled water and baked at 105 °C for 1 week. The acid-treated samples were denoted AC_N-HA, AC_C-HA and AC_Y-HA, respectively.

Table 1
Manufacturer's specifications of activated carbons used

Specifications	Norit[a]	F-400[b]	YUB[c]
Material	Coconut shell	Bituminous coal	Wood
Mean particle size (mm)	1.4	1.2	1.2
Total surface area (m^2/g)	950	950	980
Iodine number (mg/g)	1020	1000	1000
Hardness (Ball-Pan, %min)	95	95	>.98%
Abrasion number (%wt min)	60	75	94
Bulk density (g/mL)	0.49–0.52	0.36–0.38	0.44–0.48
Ash content	<3%	6.0	<3%

[a] Norit, Amersfoort, The Netherlands.
[b] Calgon Corp., Pittsburgh, PA.
[c] China Carbon Corp., Taipei, Taiwan.

2.2. Characterization of carbons

The pore size distribution, BET surface area, macropore volume V_{macro}, mesopore volume V_{meso} and micropore volume V_{micro}, of the samples were determined from the N_2 adsorption and desorption isotherms that were measured at 77 °K using an adsorption apparatus (ASAP 2010, Micromeritics Co., Georgia, USA). The pore size distribution and V_{meso} were evaluated by applying the Dollimore–Heal method [18] to desorption isotherm, whereas the *t*-plot approach [19] was adopted to estimate V_{micro}. The Dubinin–Astakhov equation [20] was applied to the CO_2 adsorption data that were measured at 25 °C to determine the V_{macro} of carbons.

The surface chemistry of carbons was determined by mass titration methods in 0.1 M NaCl. Acid/base depletion from HCl/NaCl and NaOH/NaCl solutions was performed on each sample to determine the acid/base characteristics of the carbons [21]. The oxygen content of the carbons was measured using hydrogen reduction [22].

2.3. Kinetic adsorption measurements

The kinetic adsorption of BrO_3^- was performed in a rotary tumbler at a rate of rotation of 120 rpm. A suitable dose of carbon was introduced into 100 mL amber glass bottles. The carbon that was used in the kinetic tests was soaked overnight in Milli-Q water (buffered with 10 mM Na_2HPO_4/H_3PO_4, adjusted to pH 7.5 by adding HCl) to promote the wetting of the carbon surface and the internal pore structure. Then, 200 μL of a 100 mg/L solution of BrO_3^- was injected until the BrO_3^- concentration in the bottle was 200 μg/L. The bottles were filled with BrO_3^- solution to eliminate headspace and capped with Teflon septum caps. Then, they were placed on a rotary tumbler with samples that were obtained at predetermined intervals over a period of 24 h. Samples were filtered through pre-washed 0.45 μm filters to

remove activated carbon and the residual BrO_3^- concentration was determined.

2.4. Adsorption isotherm measurements

The equilibrium adsorption isotherms of BrO_3^- from a synthetic solution on activated carbon were obtained at 25 ± 1 °C using the bottle-point approach. Various amounts of carbon were weighed and added to 18 amber glass bottles, to each of which was added 100 mL of BrO_3^- solution (200 μg/L). A non-porous carbon (inactivated coal) was also used to yield a specific surface area for calibration. The synthetic solutions were prepared using Milli-Q water, and were buffered by adding 10 mM Na_2HPO_4/H_3PO_4 at pH 7.5. The water was added to the amber glass bottles. Two hundred microliter of a 100 mg/L solution of BrO_3^- was injected until the BrO_3^- concentration in the bottle was 200 μg/L. The bottles were placed in a rotary tumbler in a temperature-controlled room at 25 ± 1 °C, and rotated at 120 rpm for 24 h.

2.5. Analyses

BrO_3^- and Br^- concentrations were obtained using an ion chromatograph (Model 2000i, Dionex, CA) that was equipped with IonPac AS9-HC analytical/AG9-HC guard columns and an anion micromembrane suppressor. The eluent solutions were 20 mM $Na_2B_4O_7$ and 18 mM NaOH. The minimum detection limits (MDL) for BrO_3^- and Br^- were 1.2 and 4.5 μg/L, respectively. Calibrations were performed before each series of samples was analyzed, and the control standard (10 μg-BrO_3^-/L and 25 μg-Br^-/L) was confirmed every 10 injections.

3. Results and discussion

3.1. Effect of carbon characteristics on adsorption kinetics

Fig. 1 displays typical N_2 adsorption–desorption isotherms for sample of coconut shell (AC_N), bituminous coal (AC_C) and wood-based (AC_Y) ACs. The development of mesopores is clearly verified by the shapes of the isotherms. Table 2 presents the porous characteristics of the ACs, as determined from the isotherms. Wood-based AC_Y carbon has a high V_{meso} value of

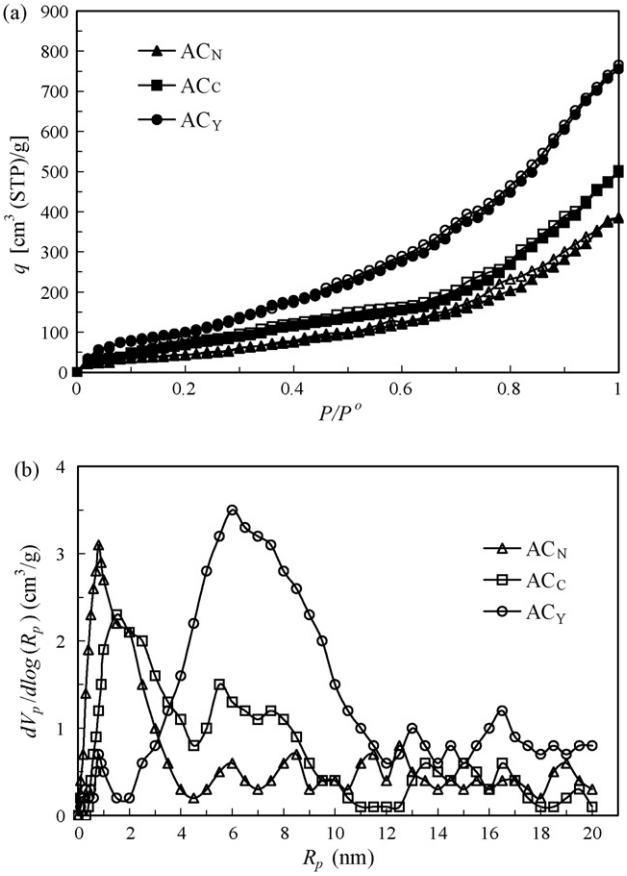

Fig. 1. (a) Nitrogen adsorption–desorption isotherms of ACs and (b) pore size distributions of ACs.

up to 0.76 cm^3/g – much higher than those of AC_N and AC_C. Fig. 1b compares the pore size distributions of three ACs, where R_p and V_p are the pore radius and the pore volume, respectively. Mesopores in the range $2 < R_p < 12$ were abundant in AC_Y carbon.

Table 2 also presents the chemical characteristics, bulk oxygen content and pH_{zpc}, of each form of carbon. Clearly, the wood-based carbon (AC_Y) contains more oxygen than the coconut- and coal-based carbons. The oxygen content of the heat-treated samples of AC_Y carbon declines as the reduction temperature increases to 950 °C, and the oxygen content is sim-

Table 2
Porous and surface properties of activated carbons

Carbon	V_{meso} (cm^3/g)	V_{micro} (cm^3/g)	Oxygen content (%)	pH_{zpc}	Acid (meq/g)	Basic (meq/g)	Hydroxyl groups (meq/g)
AC_N[a]	0.089	0.812	3.5	5.2	0.18	0.23	0.07
AC_N-HA[b]	0.072	0.816	–	–	0.20	0.16	0.03
AC_C	0.175	0.689	4.3	5.8	0.21	0.57	0.08
AC_C-HA	0.159	0.693	–	–	0.26	0.22	0.03
AC_Y	0.760	0.242	11.5	4.1	0.23	0.71	0.26
AC_Y-HA	0.736	0.277	–	–	0.44	0.33	0.11
AC_Y-T550[c]	0.773	0.231	6.9	–	–	–	0.19
AC_Y-T950[d]	0.781	0.194	4.2	–	–	–	0.10

[a] Virgin carbon.
[b] Acid washed with 6N HNO_3.
[c] Thermal reduction at 550 °C.
[d] Thermal reduction at 950 °C.

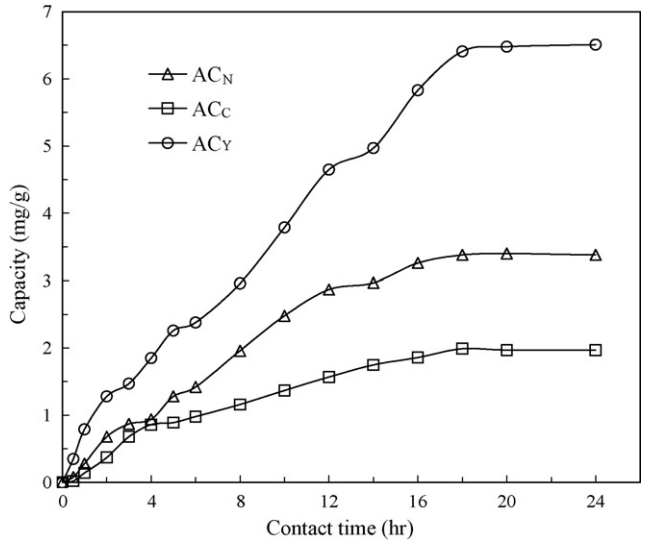

Fig. 2. Kinetic plots of BrO_3^- adsorption by three selected ACs.

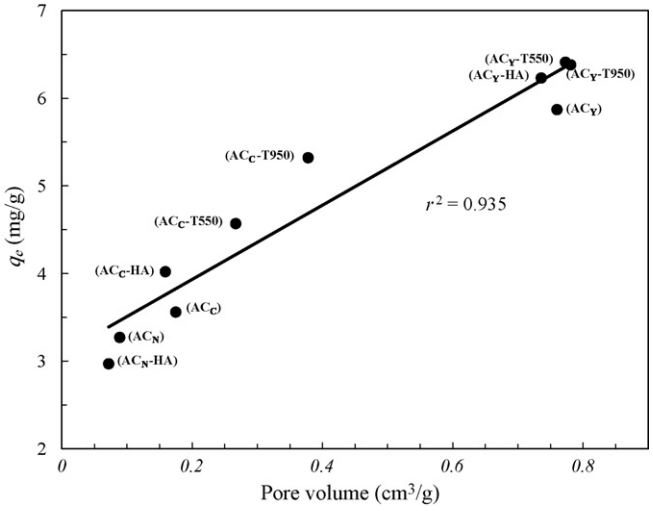

Fig. 3. Correlation of q_e of adsorbed BrO_3^- with mesopore volumes.

ilar to that in the hydrophobic carbons of samples AC_N and AC_C. Surface charge titration analyses of these carbons reveal that the AC_Y carbon has a lower pH_{zpc} (4.1) than the other carbons, indicating that the species and amount of ionizable groups on these carbons vary. The variation in surface charge with pH also indicates that the quantity and quality of surface ionizable groups vary markedly with the amount of these carbons. The variation thereof for the wood-based carbon markedly exceeds those of the coal- and coconut-based carbons. The net surface charges on AC_C carbon (-0.11 ± 0.24 meq/g) and AC_Y carbon (-0.68 ± 0.82 meq/g) are mainly negative, whereas AC_N carbon (0.07 ± 0.25 meq/g) is mostly positive in the pH range 6–8.

Fig. 2 presents the batch kinetic removal curves of amounts adsorbed (q_e) versus contact time (t) for the three carbons of interest with a BrO_3^- single component. Clearly, 20 h is enough for all of the adsorption systems to reach equilibrium. The kinetics of adsorption of BrO_3^- on the three carbons is currently described using three kinetic models – pseudo-first-order, pseudo-second-order and intraparticle diffusion models – to identify the potential rate-controlling steps in this work. The validity of the three models can be determined using the linear plots of $\log(q_e - q)$ versus t (Eq. (1)), t/q_t versus t (Eq. (2)), and q_t versus $t^{1/2}$ (Eq. (3)).

$$\log(q_e - q_t) = \log q_e - \frac{k_1}{2.303} t \tag{1}$$

where q_e and q_t are the amounts of BrO_3^- adsorbed at equilibrium and at time t, respectively, and k_1 is the equilibrium rate constant of pseudo-first-order adsorption.

$$\frac{t}{q_t} = \frac{1}{k_2 q_e^2} + \frac{1}{q_e} t \tag{2}$$

where k_2 is the equilibrium rate constant of pseudo-second-order adsorption.

$$q_t = k_p t^{1/2} \tag{3}$$

where k_p is the intraparticle diffusion rate constant [23–25].

Table 3 presents the normalized standard deviation (σ_v, %), the sum of squared errors (SSE), and the correlation coefficient to compare quantitatively the fitness of the models. Confidence limits are also determined for all three kinetic models. The calculated values reveal that the size of the confidence interval is smaller for intraparticle diffusion at the 1% level of acceptance than in other kinetic models. Additionally, Table 3 indicates that the values of σ_v and SSE for pseudo-first-order and pseudo-second-order kinetics markly exceed those in the intraparticle diffusion model. The fact that the intraparticle diffusion model is strongly consistent the experimental data suggests that the adsorption of BrO_3^- on activated carbon is diffusion-controlled.

The AC_Y carbon had a markrdly higher diffusion rate than the other two carbons (Table 3). Since it also has a higher V_{meso}, the mesopores of carbon can be reasonably assumed to be important to the adsorption of BrO_3^-. However, the extent of BrO_3^- removal (adsorption capacity) varied significantly from carbon to carbon, ranging from 73% to almost complete removal at an initial BrO_3^- concentration of 200 μg/L. The data were analyzed to determine carbon properties, especially carbon porosity and pore size distribution—to improve our understanding of the kinetic adsorption parameters in Table 2 and Fig. 1. In contrast with these and other published findings concerning the effect of pore volume on BrO_3^- adsorption [14], Fig. 3 plots the correlation between the maximum main amount of adsorbed BrO_3^- and the mesopore volumes of each AC. Give the correlation indicated by the authors' earlier work, the fact that the total pore volumes of AC contribute to the BrO_3^- adsorption process, with a 76% linear correlation, cannot be neglected. However, the mesopores alone yield a correlation of 93%. The strong correlation indicates that any selection of an activated carbon for removing BrO_3^- must consider the mesopore volume fraction.

3.2. Effect of particle size on adsorption kinetics

At a fixed carbon concentration, activated carbon (AC_Y) particles were milled to size of 0.2–0.5 μm (>400 mesh, main diameter = 0.35 μm, abbrev. AC_{Ym1}) to remove BrO_3^-; they

Table 3
Comparison of kinetic parameters for the adsorption of bromate on three selected ACs

Carbon	First-order kinetic model					Second-order kinetic model					Intraparticle diffusion				
	q_e (mg/g)	k_1 (1/h)	r^2	σ_v (%)	SSE	q_e (mg/g)	k_2 (g/mg h)	r^2	σ_v (%)	SSE	$q_{e,exp}$(mg/g)	k_p (mg/g h$^{1/2}$)	r^2	σ_v (%)	SSE
AC_N	4.7	0.188	0.92	12.35	3.19	3.5	0.019	0.92	2.43	6.73	16.9	0.136	0.96	0.24	1.85
AC_C	6.6	0.265	0.93	16.67	1.82	8.5	0.024	0.91	12.10	2.89	21.2	0.125	0.95	0.32	2.19
AC_Y	12.0	0.751	0.94	5.91	2.77	16.6	0.031	0.97	6.60	4.78	94.8	0.561	0.97	0.11	0.75

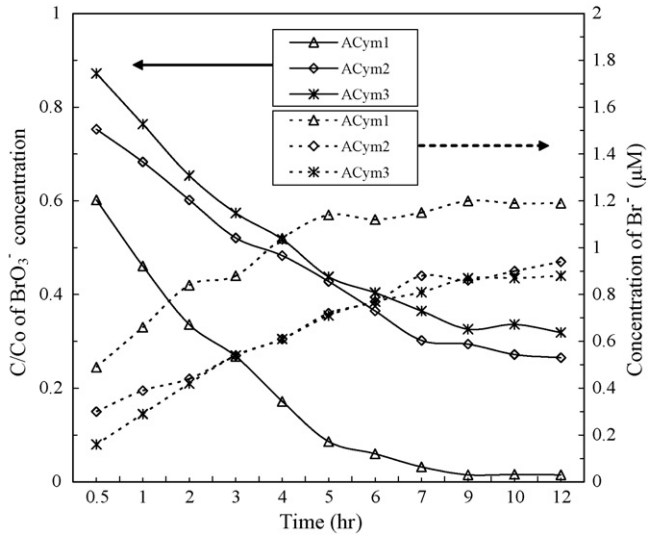

Fig. 4. Evolution of dimensionless remaining concentration of BrO_3^- (solid lines) and concentration of Br^- released (dashed lines) for variously sized AC particles.

were compared with large AC particles, with diameters from 53 to 74 μm (230–300 mesh, main diameter = 65.5 μm, abbrev. AC_{Ym2}) and from 470 to 681 μm (20–30 mesh, main diameter = 575 μm, abbrev. AC_{Ym3}). Fig. 4 plots the concentration of BrO_3^- with time and the release of bromide (Br^-) by AC adsorption–reduction. The initial rates of degradation of AC_{Ym1} per unit mass of BrO_3^- markedly exceeded those of AC_{Ym2} or AC_{Ym3}. Almost 55% of the BrO_3^- was removed using AC_{Ym1} as the adsorbent–reductant in the first hour. However, in the presence of the largest AC particles, only 20–25% of BrO_3^- was removed. In particular, as presented in Fig. 4, the release of bromide ions (Br^-) during the degradation of BrO_3^- was more rapid when the AC_{Ym1} was the adsorbent.

Fig. 5 plots the global rate constants (K_T) obtained under steady-state conditions (after 12 h of operation) for arithmetic average particle sizes of 0.35, 65.5 and 575 μm. The data reveal that pore diffusion influences the overall BrO_3^- reac-

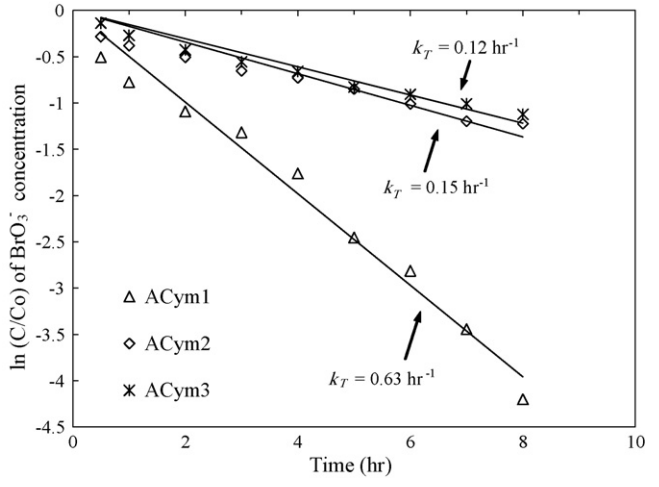

Fig. 5. Evolution of rate constant (k_T) of total removal of BrO_3^- for various AC particle sizes.

tion rate: a drop in particle size diameter from 575 to 0.35 μm increases the steady-state rate constant from 0.12 to 0.63 h^{-1}. The higher BrO_3^- uptake and rate constants of smaller particles are attributable to greater accessibility to pores and greater surface area for bulk adsorption per unit weight of carbon. The shorter equilibrium time for smaller particles may follow from the dominance of intraparticle diffusion in smaller particles. The breaking up of large particles opens some tiny sealed channels, which may then become available for adsorption, so the adsorption by smaller particles is greater than that by larger particles.

3.3. Effect of pore size on adsorption isotherms

Fig. 6 plots the adsorption isotherms with carbons and BrO_3^- solution in buffered Milli-Q water. The isotherms were interpreted using the Langmuir isotherm model, which is expressed as:

$$\frac{1}{q_e} = \frac{1}{q_m} + \frac{1}{q_m K_L}\frac{1}{c} \quad (4)$$

where q_e and c are the concentrations of BrO_3^- in the activated carbon and solution, respectively, q_m represents the maximum sorption capacity, and K_L is a constant that is related to the adsorption energy (equilibrium constant for adsorption of BrO_3^-). Table 4 summarizes the calculated monolayer equivalent amount adsorbed and the mean maximum amount adsorbed by each carbon. The agreement between the sets of data is generally good. In fact, a large difference between BrO_3^- adsorptions is evident, indicating the molecular sieve effect of activated carbons. Table 2 reveals that all carbons other than AC_Y carbon have only a small mesopore volume. Fig. 7 indicates the extent to which mesoporous wool-based carbons exhibit a greater affinity for BrO_3^- during adsorption from pure water at pH 7.5 than do microporous coconut- and coal-based carbons. This result is similar to Fig. 3, which indicates a strong correlation between the maximum adsorbed amount (q_m) and the mesopore volumes

Table 4
Isotherm parameters for tested carbons

Carbon	q_m (mg/g)	K_L (L/mg)	r^2
AC_N	16.2	2.01	0.92
AC_C	26.3	1.15	0.91
AC_Y	90.9	0.44	0.94
NC	10.5	2.72	0.89

of each AC. The amounts of BrO_3^- that are adsorbed by the microporous coconut- and coal-based carbons are very similar to the amount adsorbed by nonporous carbon black (NC), even at a high carbon dose of 1000 mg/L, indicating no increase in BrO_3^- adsorption capacity. Therefore, the micropores in these carbons are posited to present only a nominal internal surface for adsorption.

3.4. Effect of chemical characteristics on adsorption isotherms

The effect of surface chemistry on the adsorption of BrO_3^- by activated carbon is studied by reducing the oxygen content of AC_Y carbon without changing the pore volume (Table 2). In making these measurements, BrO_3^- is exposed to activated carbons with increasing hydrophobic character, but a space of constant volume is available for adsorption. In the aqueous phase, surface oxygen groups are important to the adsorption of BrO_3^-. In particular, increasing the amount of carboxylic groups on the surface promotes the formation of water clusters and the removal of π electrons from the basal planes [26], weakening interactions with ionic adsorbates. The effect of chemistry (oxygen content) is evident at low adsorptive concentrations. Therefore, the amount adsorbed by virgin AC_Y carbon (oxygen content = 11.5%) is markedly lower than the amounts adsorbed by the two heat-treated carbons (oxygen content = 6.9 and 4.2%, respectively).

The surface chemical groups are classified according to their acid–base character (Table 2). At a fixed pH (7.5), the

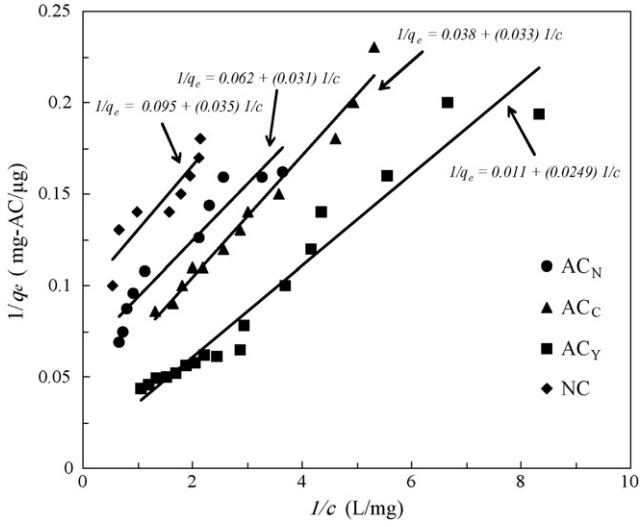

Fig. 6. Langmuir adsorption isotherms of BrO_3^- on three selected ACs.

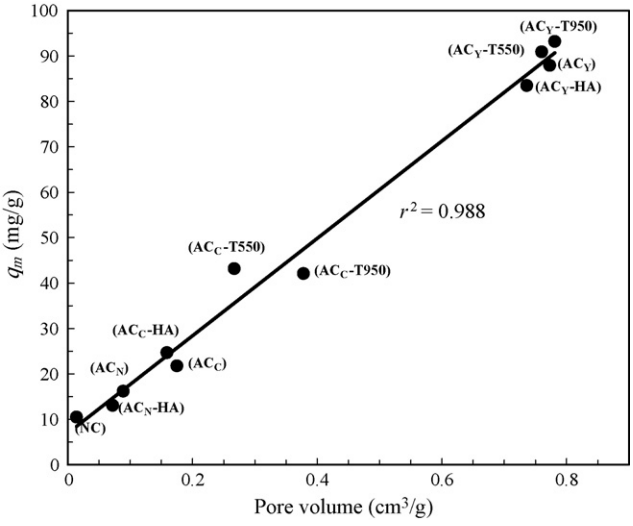

Fig. 7. Correlation of q_m of adsorbed BrO_3^- with mesopore volume.

properties of these groups were strongly correlated with the adsorption of BrO_3^-. The virgin carbon, which was more effective than the acid-washed carbons in removing BrO_3^-, has many more basic groups. The infrared spectra of these carbons reveal that the raw carbons contain more hydroxyl groups than the acid-washed carbons (data not shown). Weak ionic interactions typically participate in the adsorption of BrO_3^- by activated carbon surfaces by bonding between the negatively charged side of the anion and the positively charged carbon surface. Based on the discussion of the effects of carbon surface chemistry on BrO_3^- adsorption, both the physical and the chemical effects are suggested simultaneously to influence adsorption.

4. Conclusion

The adsorption kinetics and isotherms of BrO_3^- on activated carbon reveal that the characteristics of activated carbon influence the capacity for the adsorption–reduction of BrO_3^-. These properties were found to affect the amount of BrO_3^- converted. Analysis of various properties of AC at a treatment plant indicated that the carbons with the largest mesopores adsorbed the most BrO_3^-. A comparison of the kinetic models and the overall adsorption capacity was best described by the intraparticle diffusion model in these three carbon cases. The intraparticle diffusion played a significant role that indicated the importance of selecting the carbon porosity and pore size to accelerate BrO_3^- adsorption. The functional group on the carbon surface importantly determined its capacity to adsorb BrO_3^-. The carbons with more basic surface groups and higher pH_{zpc} had a higher BrO_3^- adsorption capacity, suggesting that protons are adsorbed on the available surface hydroxyl groups or phenolic groups under typical pH conditions. To achieve effective BrO_3^- removal from an aqueous solution, the combination of mesopore volumes and surface chemistry should be considered as the principal criterion for adsorbent selection.

Acknowledgement

The authors would like to thank the National Science Council of the Republic of China, Taiwan, for financially supporting this research under Contract no. NSC-93-2211-E-241-005.

References

[1] Y. Kurokawa, Y. Hagashi, Y. Maekawa, M. Takahashi, T. Kokubo, Induction of renal cell tumors in F-344 rats by oral administration of potassium bromate, a food additive, Gann 73 (1982) 335–341.
[2] W.R. Haag, J. Hoigne, Ozonation of bromide containing waters: kinetics of formation of hypobromous acid and bromate, Environ. Sci. Technol. 17 (1983) 261–267.
[3] D.C. Wolf, L.M. Crosby, M.H. George, S.R. Kilburn, T.M. Moore, R.T. Miller, A.B. DeAngelo, Time- and dose-dependent development of potassium bromate-induced tumors in male Fischer 344 rats, Toxicol. Pathol. 26 (1998) 724–729.
[4] U. von Gunten, J. Hoignè, Bromate formation during ozonation of bromide-containing waters: Interaction of ozone and hydroxyl radical reactions, Environ. Sci. Technol. 28 (1994) 1234–1242.
[5] W.H. Glaze, H.S. Weinberg, J.E. Cavanagh, Evaluating the formation of brominated DBPs during ozonation, J. Am. Water Works Assoc. 85 (1993) 96–103.
[6] S.W. Krasner, W.H. Glaze, H. Weinberg, P. Daniel, I. Najm, Formation and control of BrO_3^- during ozonation of waters containing bromide, J. Am. Water Works Assoc. 85 (1993) 73–80.
[7] M.S. Siddiqui, G.L. Amy, Factors affecting DBP formation during ozone-bromate reactions, J. Am. Water Works Assoc. 86 (1994) 63–72.
[8] D. Delker, G. Hatch, J. Allen, B. Crissman, M. George, D. Geter, S. Kilburn, T. Moore, G. Nelson, B. Roop, R. Slade, A. Swank, W. Ward, A. DeAngeol, Molecular biomarkers of oxidative stress associated with bromate carcinogenicity, Toxicology 221 (2006) 158–165.
[9] WHO, Bromate in Drinking Water: Background Document for of WHO Guidelines for Drinking-water Quality, WHO, 2005, pp. 4–10.
[10] M.S. Siddiqui, W. Zhai, G.L. Amy, C. Mysore, Bromate ion removal by activated carbon, Water Res. 30 (1996) 1651–1660.
[11] M.J. Kirisits, V.L. Snoeyink, J.C. Kruithof, The reduction of bromate by granular activated carbon, Water Res. 34 (2000) 4250–4260.
[12] M.L. Bao, O. Griffini, D. Santianni, K. Barbieri, D. Burrini, F. Pantani, Removal of bromate ion from water using granular activated carbon, Water Res. 33 (1999) 2959–2970.
[13] M. Asami, T. Aizawa, T. Morioka, W. Nishijima, A. Tabata, Y. Magara, Bromate removal during transition from new granular activated carbon (GAC) to biological activated carbon (BAC), Water Res. 33 (1999) 2797–2804.
[14] J. Miller, V.L. Snoeyink, S. Harrell, The effect of granular activated surface chemistry on bromate reduction, in: R.A. Minear, G.L. Amy (Eds.), Disinfection by-products in Drinking Water Treatment—The Chemistry of their Formation and Control, CRC Press, Boca Raton, FL, 1996, pp. 293–309.
[15] M.L. Studebaker, The chemistry of carbon black and reinforcement, Rubber Chem. Technol. 30 (1957) 1400–1483.
[16] D. Graham, Characterization of physical adsorption systems-III: The separate effects of pore size and surface acidity upon the adsorbent capacities of activated carbons, J. Phys. Chem. 59 (1955) 896–900.
[17] R. Considine, R. Denoyel, P. Pendleton, R. Schumann, S.H. Wong, The influence of surface chemistry on activated carbon adsorption of 2-methylisoborneol from aqueous solution, Colloids Surf. A: Physicochem. Eng. Aspects 179 (2001) 271–280.
[18] D. Dollimore, G.R. Heal, An improved method for the calculation of pore size distribution from adsorption data, J. Appl. Chem. 14 (1964) 109–114.
[19] B.C. Lippens, J.H. de Boer, Pore system *n* catalysts V: the t-method, J. Catal. 4 (1965) 319–323.
[20] M.M. Dubinin, V.A. Astakhov, Description adsorption equilibria of vapors on zeolites over wide ranges of temperature and pressure, Adv. Chem. Ser. 102 (1971) 69–85.
[21] S.S. Barton, M.J.B. Evans, E. Halliop, J.A.F. MacDonald, Acidic and basic sites on the surface of porous carbon, Carbon 35 (1997) 1361–1366.
[22] M.C. Carlos, F.P.C. Agustin, M.H. Francisco Jr., C.M. Francisco, J.L.G. Fierro, Influence of carbon-oxygen surface complexes on the surface acidity of tungsten oxide catalysts supported on activated carbon, Carbon 41 (2003) 1157–1167.
[23] H. Sontheimer, J.C. Crittendan, R.S. Summers, Activated Carbon for Water Treatment 2nd, DVGW-Forschungsstelle, Engler-Bunte-Institut Universität Karlsrube, Germany, 1989.
[24] F.C. Wu, R.L. Tseng, R.S. Juang, Adsorption of dyes and phenols from water on the activated carbons prepared from corncob wastes, Environ. Technol. 22 (2001) 205–213.
[25] P.K. Malik, Use of activated carbons prepared from sawdust and rice-husk for adsorption of acid dyes: a case study of Acid Yellow 36, Dyes Pigment 56 (2003) 239–249.
[26] I.I. Salame, T.J. Bandose, Role of surface chemistry in adsorption of phenol on activated carbon, J. Colloid Interface Sci. 264 (2003) 307–312.